water

MDPI

Article

Spatial Distribution Characteristics and Genetic Mechanism of the Metasilicate-Rich Groundwater in Ji'nan Rock Mass Area, Shandong Province, China

Meng Xu [1], Caiping Hu [2,*], Lixin Zhu [3], Guangzeng Song [1], Wenquan Peng [1], Shijiao Yang [1] and Jinyu Song [1]

[1] No. 1 Institute of Geology and Mineral Resources of Shandong Province, Shandong Provincial Bureau of Geology & Mineral Resources, Ji'nan 250100, China
[2] Shandong Provincial Geo-Mineral Engineering Exploration Institute, Shandong Provincial Bureau of Geology & Mineral Resources, Ji'nan 250014, China
[3] China Geological Survey, Beijing 100037, China
* Correspondence: caipinghu126@126.com

Abstract: Metasilicate-rich groundwater could meet the high demand of the international community for high-quality water. In order to comprehensively analyze the genetic mechanism of metasilicate-rich groundwater, and help human communities effectively exploit and utilize high-quality water resources, taking the Ji'nan rock mass area as an example, this study carried out systematic research on the spatial distribution and genetic mechanism of the metasilicate-rich groundwater Based on the regional hydrogeological conditions, the influencing factors on the spatial distribution characteristics of the metasilicate-rich groundwater in the study area were systematically sorted out by means of petrogeochemistry, hydrochemistry, and chemical weathering index analysis, and the accumulation mechanism of the metasilicate-rich groundwater was discussed from the perspective of water-rock interaction. The results show that: (1) On the northwest side and part of the northeast side of Ji'nan rock mass, the metasilicate content of the groundwater samples exceeded 25 mg/L; the metasilicate content on the south, west, and east sides were relatively low; (2) Ji'nan rock mass is mainly composed of gabbro easily weathered, with high SiO_2 content and high weathering degree showing obvious characteristics of desilication. FeS_2 developing along the contact zones between the rock mass and surrounding rocks was easily oxidized to form H_2SO_4, which enhanced the solubility of silicate minerals in the groundwater. Ji'nan rock mass was located in the low-lying position of the monocline structure, which presented better water conservation and recharges conditions. The above factors resulted in the metasilicate-rich groundwater accumulating in the area of Ji'nan rock mass and showed different spatial distribution characteristics.

Keywords: Ji'nan rock mass; metasilicate-rich groundwater; water-rock interaction; solution of silicate rock; human factor

Citation: Xu, M.; Hu, C.; Zhu, L.; Song, G.; Peng, W.; Yang, S.; Song, J. Spatial Distribution Characteristics and Genetic Mechanism of the Metasilicate-Rich Groundwater in Ji'nan Rock Mass Area, Shandong Province, China. *Water* **2023**, *15*, 713. https://doi.org/10.3390/w15040713

Academic Editors: Yong Xiao, Jianping Wang and Jinlong Zhou

Received: 2 December 2022
Revised: 3 February 2023
Accepted: 3 February 2023
Published: 11 February 2023

1. Introduction

The global demand for water has grown approximately six-fold in the last century [1,2]. Continued population growth and climate change in the 21st century will have a severe impact on global water resources [3,4]. Water scarcity occurs in many countries, particularly in the Mediterranean, Middle Eastern, and African countries, and many of these countries are confronted with a crucial combination of a severe lack of an increasing demand for high-quality water [5]. Groundwater has significant advantages of spatial-temporal availability compared to surface water, and it is the most important water resource for more than half of the global population [6,7]. Consequently, high-quality groundwater has played and will continue to play an essential role in social, economic, agricultural and industrial development for the international community.

The metasilicate-rich groundwater is one important kind of high-quality groundwater, which has a significant effect on softening human blood vessels, and relieving arteriosclerosis and heart disease in medicine [8]. Because catering to the rapid demand for high-quality groundwater and being beneficial for human health, metasilicate-rich groundwater has become a hot topic in hydrogeology research.

The hydrochemical formation of metasilicate-rich groundwater is affected by multiple factors, such as geological structure, lithofacies composition, hydrodynamic conditions, and hydrochemical characteristics [9–11]. Due to its important economic and medical value, its genetic mechanism has attracted the attention of many scholars. However, most of the previous studies focused on the influence of extrusive rocks (especially basalt) on the formation of metasilicate, or focused on the discussion about the metasilicate from the perspective of hydrochemical evolution. The research on how the intrusive rocks, geochemical characteristics, and weathering of surrounding rocks affected the metasilicate-rich groundwater from the perspective of water-rock interaction was relatively few, which has limited the effective exploration and utilization of metasilicate-rich groundwater. In the Ji'nan rock mass area, parts of the groundwater are enriched with H_2SiO_3. Moreover, the intrusive rocks are widely distributed, with various mineral types, structural and weathered fractures, and metal sulfide deposits are widely distributed. These have determined the water-rock interaction processes of the H_2SiO_3 enrichment in groundwater.

Taking the Ji'nan rock mass area as an example, this study discusses the distribution characteristics and formation mechanism of the metasilicate-rich groundwater from the perspective of analyzing the coupling relationship between rock weathering and water chemical formation. It not only comprehensively considers the potential influencing factors of the metasilicate-rich groundwater, but also contributes to the effective exploitation and utilization of the metasilicate-rich groundwater, and helps meet the highing demand of the international community for high-quality water.

2. Geological Background

Located in the northern wing of the Taishan Dome, Ji'nan is a north-dipping monoclinic structure dominated by Paleozoic carbonate strata. The southern is mountainous, with exposed limestones distributing continuously, and acts as the recharge area of the groundwater. The central hills become slope, and the main lithology includes Cambrian limestone, shale, and middle and lower Ordovician limestone, and acts as the recharge-runoff area of the groundwater. The northern is the Yellow River alluvial plain, which is the buried limestone distribution area and the groundwater discharge area, where the Ji'nan Rock mass area (study area) is located (Figure 1). Ji'nan is located in the mid-latitude inland zone, and belongs to a temperate monsoon climate, with an average annual precipitation of 669.91 mm.

In the Ji'nan area, the Ordovician limestone forms the main aquifer group, and the groundwater flows from south to north. In the process of northward runoff, after encountering the barrier of Ji 'nan rock mass, part of the groundwater flows out of the surface along the faults and other weak zones to form famous Ji'nan spring groups, and part enters the deep circulation to form the geothermal field on the north of the Yellow River [12].

The study area is based on the Archean Taishan Group (Art), which is overlaid by Cambrian, Ordovician, Carboniferous, Permian, Cretaceous, Neogene and Quaternary strata from bottom to up, and the lithology mainly includes limestone, dolomite, and clastic rock. The faults in the area are mainly composed of three groups of NS, NNE, and nearly NW trending faults, such as the Sangzidian Fault, Qianfoshan Fault, etc. In the early Cretaceous, the Ji'nan rock mass was formed by the eruption of magmatic activities, mainly composed of gabbro and pyroxene monzonite [13]. At present, most of the Ji 'nan rock mass is covered by the Quaternary system, and it only appears sporadically in Yaoshan, Huashan, and Woniushan Mountains, etc. On the plane, it is roughly elliptical in the direction of EW, and the spatial form presents giant rock falx.

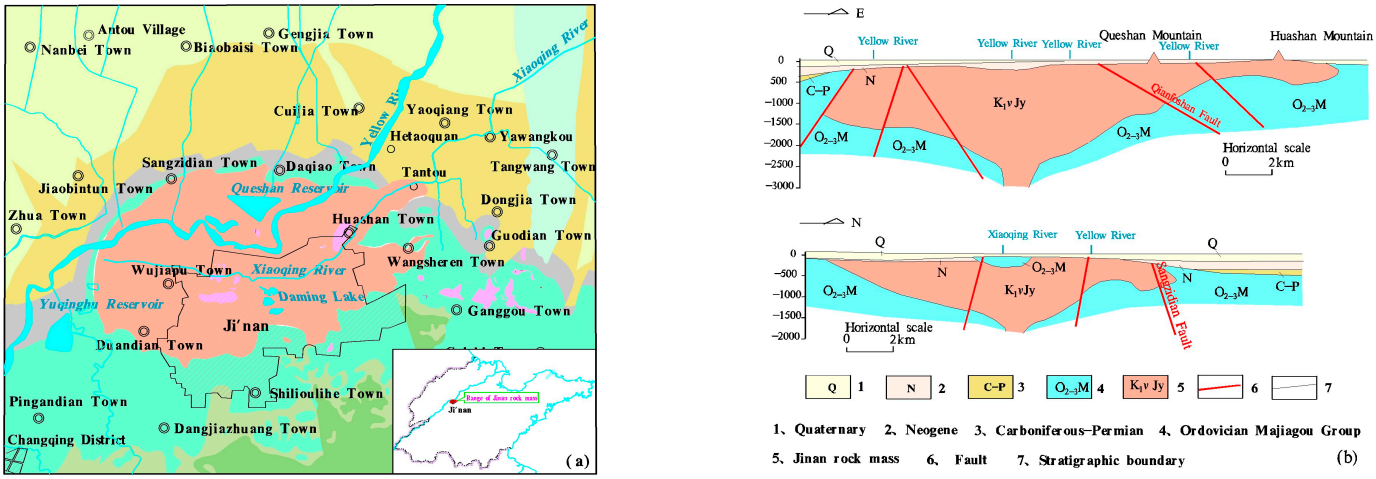

Figure 1. The geological background of the Ji'nan rock mass area. (**a**)—The location and hydrogeological conditions of Ji'nan rock mass area; (**b**)—Plane and longitudinal profile of Ji'nan rock mass.

3. Data Sources and Research Methods

Based on the collection of regional geological and hydrogeological data, 29 groundwater samples in the study area were collected successively in July 2021 from Ordovician limestone, which is a confined aqufier. The sampling points are distributed evenly in the study area (see Figure 2 for the sampling locations). The Technical Regulations on Groundwater Environmental Monitoring (2004) were strictly implemented for sampling and analysis. Each groundwater sample was collected by using two polyethylene bottles, which were cleaned, rinsed, and filtered before sampling. One bottle of the sample was added 65% nitric acid to make the pH < 2, so as to test the cationic concentration, and the other bottle of the sample was used to test anion concentration without adding nitric acid. The samples were sent to the Ji'nan Mineral Resources Supervision and Testing Center of the Ministry of Land and Resources for water quality analysis within 24 h after collection. K^+ and Na^+ were tested by inductively coupled plasma emission spectrometry, and both the detection limits were 0.01 mg/L. Ca^{2+} and Mg^{2+} were tested by ethylenediamine tetraacetate disodium titration, and the detection limits were 2 mg/L and 1 mg/L, respectively. Cl^- was tested with the silver nitrate volumetric method, the detection limit was 1 mg/L. $SO_4{}^{2-}$ was tested with the barium sulfate turbidimetric method, the detection limit was 3 mg/L. $HCO_3{}^-$ was tested by acid-base titration with a detection limit of 5 mg/L. The soluble SiO_2 was tested by a UV spectrophotometer with a detection limit of 0.1 mg/L. The error analysis of the tested results was carried out according to the principle of ion balance, which was calculated to be less than 5%.

Rock samples of different lithologies in the study area were collected and thinly sliced. According to the micropetrographic observation, 11 representative samples without alteration were selected and broken under pollution-free conditions for testing the major elements, including SiO_2, Al_2O_3, Fe_2O_3, MgO, CaO, Na_2O, K_2O, and P_2O_5. Using an X-ray fluorescence (XRF) spectrometer, the test was carried out at the Shandong Testing Center of China Metallurgical Geology Bureau. First, 0.7 g of the sample was weighed, then boric acid was added to melt the sample into a glass sheet at a high temperature, finally, the oxide content was determined on XRF. The error of the total oxide content is 1–3%.

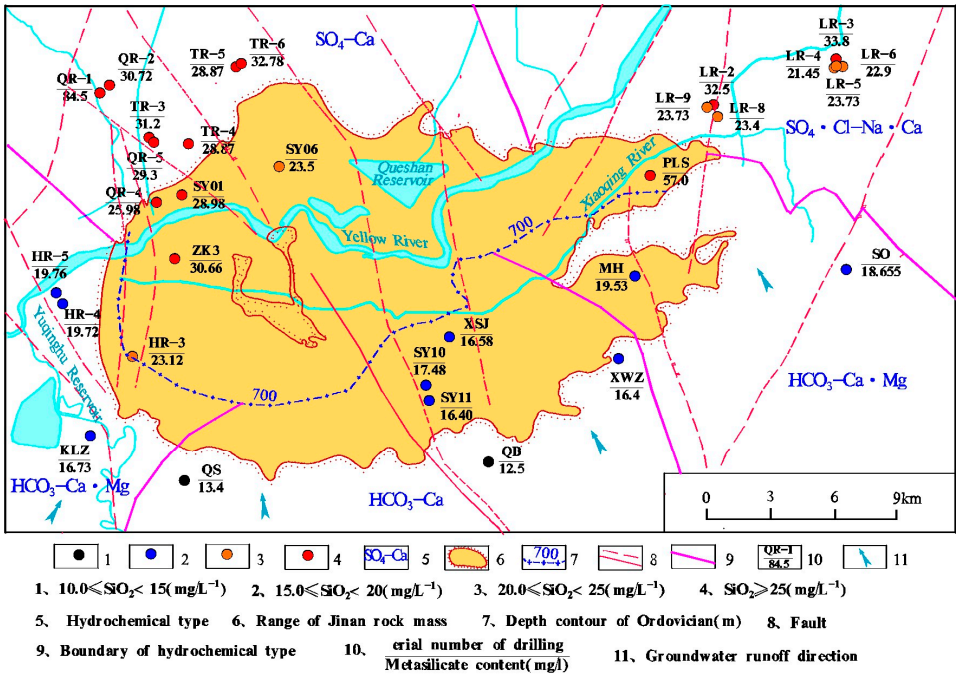

Figure 2. The metasilicate content, hydrochemical types, and distribution of the groundwater in the study area (The content of H_2SiO_3 is the concentration unit mg·L^{-1}).

4. Results and Discussion

4.1. Distribution of the Metasilicate-Rich Groundwater

Full analysis tests were conducted on the groundwater samples from 29 wells in the study area. The results showed that the content of H_2SiO_3 in 12 water samples exceeds 25 mg/L, accounting for 41.38% of the total samples. There were six samples with more than 20~25 mg/L of H_2SiO_3, accounting for 20.69%. There were 11 samples less than 20 mg/L, accounting for 37.93% (Table 1). The samples with more than 25 mg/L of H_2SiO_3 are mainly concentrated in the northwest and northeast sides of the Ji'nan rock mass, among which, nine samples are distributed on the northwest side and three samples are on the northeast side. The content of H_2SiO_3 is low in the south, west, and east sides of the rock mass, indicating that the spatial distribution of the metasilicate-rich groundwater presents regional characteristics. The content of H_2SiO_3 increased gradually from south to north, which was consistent with the groundwater runoff direction (Figure 2).

4.2. Discussion on the Origin of H_2SiO_3 Enrichment

Previous studies have shown that, only when the silicate minerals in surrounding rocks present wide distribution and strong solubility, the surrounding rocks become weathered strongly, the water-rock interaction is intense, the groundwater conservation and recharge conditions are well, then the H_2SiO_3 can be accumulated, and enriched in the groundwater [8,14]. The four above factors about the study area will be discussed in detail in the following paper to clarify the genetic mechanism of the metasilicate-rich groundwater.

4.2.1. Geochemical Conditions of Surrounding Rocks

Due to the difference in the content and the weathering sensitivity of the silicate minerals in the surrounding rocks, there are great differences in the supply degree and rate of soluble SiO_2 to the groundwater from the surrounding rocks with different geochemical characteristics [15]. The surrounding rocks of the groundwater in the study area mainly include gabbro, diorite, and carbonate rocks. In this study, 11 rock samples were collected for testing the major elements (Figure 3). The results shew that the gabbro contained large SiO_2 content, accounting for 50.1~58.5%, with an average of 52.9%. The main minerals were plagioclase and pyroxene which were easily weathered, among which the plagioclase

accounted for 42~70%, and the pyroxene accounted for 23~55%. In the diorite samples, the content of SiO_2 was 50.14%, and the main minerals were plagioclase and amphibole, among which the plagioclase, the amphibole and the pyroxene respectively accounted for 63–65%, 33–35%, and 2–3%. The carbonate rocks mainly included dolomite and limestone, and the main mineral component was dolomite or calcite, accounting for about 90%, whereas, the content of SiO_2 accounted for about 0~22.4%, with an average of 15.4%. The content of SiO_2 in carbonate rocks was low, and most of them were free quartz, which was less soluble in water, so they cannot act as the main material sources of the H_2SiO_3 in the groundwater in the study area [15,16]. Therefore, the gabbro and diorite are the main lithologies of Ji'nan rock mass, containing a large number of easily weathered silicate minerals such as plagioclase, pyroxene, and amphibole, which constitute favorable potential sources of H_2SiO_3 in groundwater.

Table 1. The H_2SiO_3 content of the groundwater samples was collected from different sides of the Ji'nan rock mass (See Figure 2 for the locations of the boreholes).

Position	Borehole Number	Content of H_2SiO_3	Borehole Number	Content of H_2SiO_3
West side	HR-5	19.76	HR-3	23.12
	HR-4	19.72		
East side	SO	18.656	MH	19.53
Northeast side	LR-2	32.5	LR-6	22.9
	LR-3	33.8	LR-8	23.4
	LR-4	21.45	PLS	57
	LR-5	23.73		
South side	QS	13.4	SY-11	16.4
	QB	12.5	XSJ	16.58
	XWZ	16.4	KLZ	16.73
	SY-10	17.48		
Northwest side	QR-2	30.72	QR-5	29.3
	TR-5	28.87	SY-1	28.98
	TR-6	32.78	SY-6	23.5
	TR-3	31.2	ZK3	30.66
	TR-4	28.87	QR-4	25.98

Note: The content of H_2SiO_3 is the concentration unit $mg \cdot L^{-1}$.

In the diagram of the water-rock interactions and the distribution of the sample points in the study area (Figure 4), almost all the sample points with more than 25 mg/L content of H_2SiO_3 are located inside or near the end-member of silicate rock, and a few sample points are located in the secondary end-member of amphibole, which proves that Ji'nan rock mass is indeed the main source of the H_2SiO_3 in groundwater. The samples with less than 25 mg/L content of H_2SiO_3 are located in the secondary end-member of amphibole or near the silicate end-member, indicating that the geochemical characteristics of the groundwater in the study area are mainly affected by silicate rocks, but less affected by carbonate rocks or evaporites.

4.2.2. Weathering Degree and Mechanism of Surrounding Rocks

Weathering and desilication of the surrounding rocks act as the basic source of H_2SiO_3 in groundwater, and the weathering degree could affect the reaction equilibrium process of the water-rock interaction [11,17]. As the source of the H_2SiO_3 in groundwater, the Ji'nan rock mass developed abundant structural fractures and weathered fractures (Figure 5a–c), and the main lithologies included easily weathered gabbro and diorite. The above two aspects comprehensively caused the surrounding rocks of the groundwater to be easily weathered, which can be proved by the spherical weathering phenomenon only formed by strong weathering (Figure 5d).

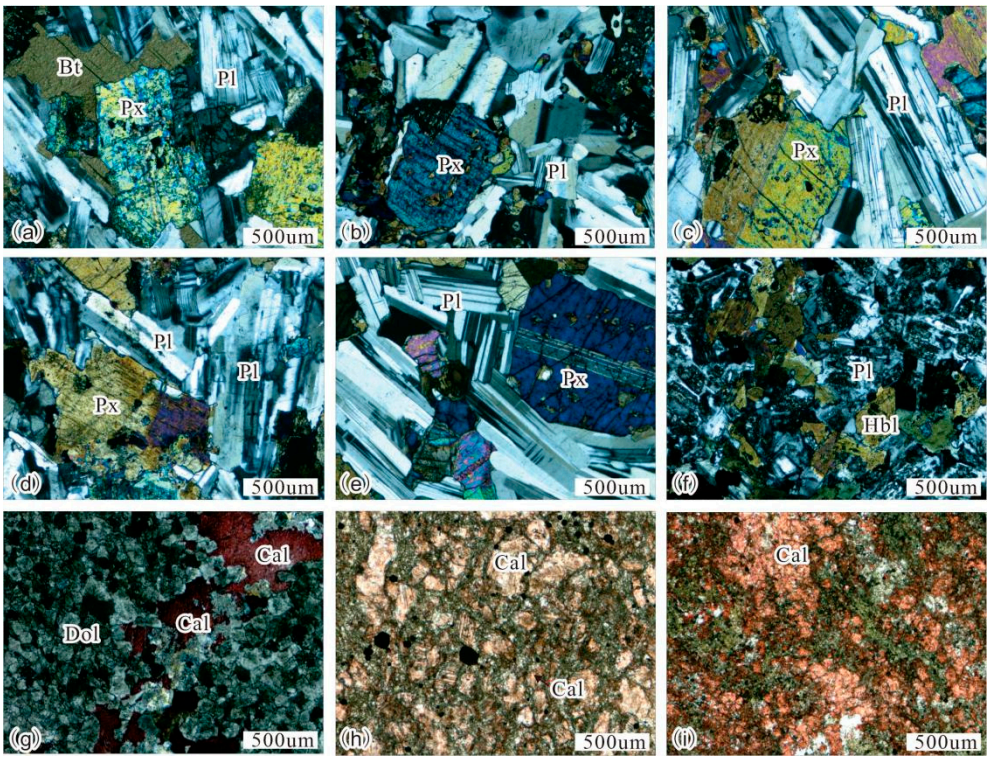

Figure 3. Microscopical features of the rock samples in the study area (**a**–**e**) are gabbros, (**f**) is diorite, and (**g**–**i**) are carbonate rocks). (**a**)—Plagioclase: 48–50%; Pyroxene: 43–45%, cleavage developed; Biotite: 3–5%; Opaque minerals: 1–2%; (**b**)—Plagioclase: 43–45%; Pyroxene: 53–55%; Mica: 1–2%; Opaque minerals: 1–2%; (**c**)—Plagioclase: 50–53%; Pyroxene: 43–45%; Mica: 2–3%; Opaque minerals: 1–2%; (**d**)—Plagioclase: 58–60%; Pyroxene: 38–40%; Biotite: 2–3%; Opaque minerals: 1–2%; (**e**)—Plagioclase: 50–53%; Pyroxene: 43–45%; Biotite: 2–3%; Opaque minerals: 1–2%; (**f**)—Plagioclase: 63–65%; Hornblende: 33–35%; Pyroxene: 2–3%; Opaque minerals: 1–2%; (**g**)—Dolomite: 95%±; Calcite: 3–5%; Quartz: 1–2%; Opaque minerals: less; (**h**)—Calcite: 90%±; Dolomite: 3–5%; Quartz: 3–5%; Tremolite: 2–3%; Diopside: little; Opaque minerals: 1%; (**i**)—Calcite: 78–80%; Dolomite: 3–5%; Quartz: 2–3%; Goldmica: 13–15%; Opaque minerals: less. Pl—plagioclase; Px—pyroxene; Hbl—amphibole; Cal—calcite; Dol—Dolomite.

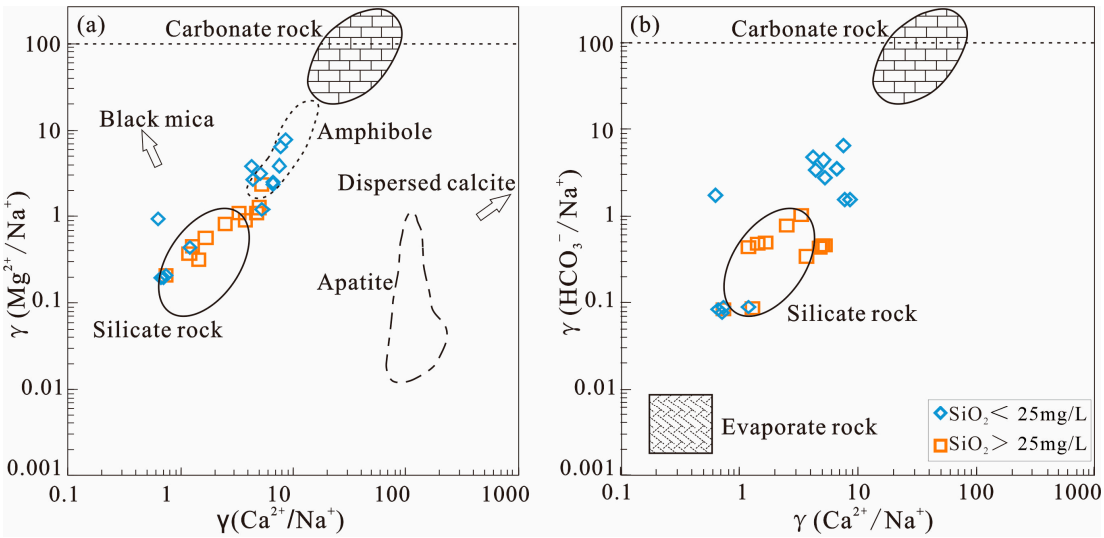

Figure 4. The relationship of Ca^{2+}/Na^{+} and Mg^{2+}/Na^{+} (**a**), Ca^{2+}/Na^{+} and HCO_3^{-}/Na^{+} (**b**) in the study area.

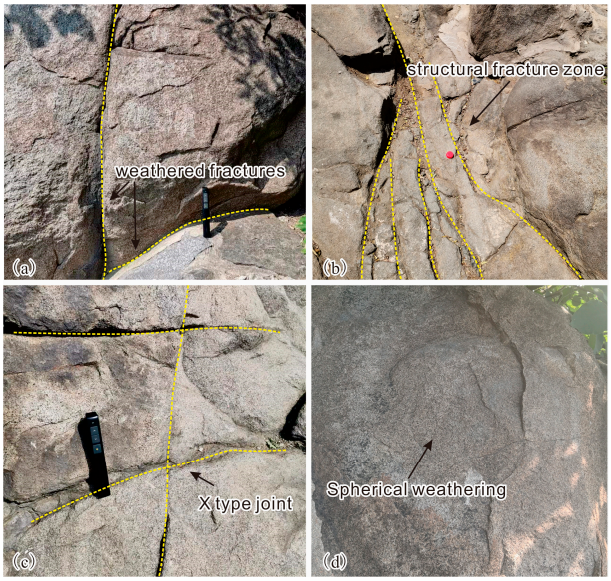

Figure 5. Fracture development and spherical weathering of the Ji'nan rock mass. (**a**)—X type joint and weathered fractures; (**b**)—Structural fracture zone; (**c**)—X type joint and weathered fissures; (**d**)—Spherical weathering.

The weathering degree of rocks is often characterized by the chemical weathering index, that is, the ratio of different specific major element oxides is used to indicate the weathering degree of the surrounding rocks [18–20]. Based on the characteristics of main lithology and major elements of the rock mass, and referring to the methods adopted by predecessors in studying the weathering degree of magmatic rocks [21–23], this study selected index of lateralization (IOL) and chemical alteration index (CIA) to quantitatively characterize the weathering mechanism and degree of Ji'nan rock mass. The two weathering indexes present high sensitivity to rock weathering, and the calculation formula is as follows respectively:

$$\text{IOL } [(Al_2O_3 + Fe_2O_3)/(SiO_2 + Al_2O_3 + Fe_2O_3)] \times 100 \quad (1)$$

$$\text{CIA } [Al_2O_3/(Al_2O_3 + CaO^* + Na_2O + K_2O)] \times 100 \quad (2)$$

note: The IOL index was calculated using the mass fraction of oxide; while the CIA index was calculated using the molecular mole number of oxide; CaO* refers to the molar content of the silicate minerals, excluding the CaO content of carbonate minerals. Since the molar ratio of CaO and Na_2O in silicate is usually 1:1, when the molar number of CaO is greater than the molar number of Na_2O, the molecular mole of CaO* is equal to that of Na_2O to carry out the calculation, and when the molar number of CaO* is less than that of Na_2O, the molar number of CaO* is equal to that of CaO when used to calculate.

The IOL index indicates the process that Al_2O_3 and Fe_2O_3 replace SiO_2 in silicate minerals, and the larger the value is, the lower the weathering degree will be. CIA index is the mole percentage ratio between the oxides of alkali metal elements K, Ca, and Na, which are easy to migrate, and the oxides of Al, which are difficult to migrate, during the process of rock weathering. CIA is used to characterize the chemical weathering intensity of the rocks, and the larger the index value is, the stronger the weathering effect will be [24].

By using the above two calculation methods, combined with the tested data of the major elements of Ji'nan rock mass (Table 2), 8 groups of gabbro and diorite samples were randomly selected to calculate the chemical weathering index of Ji'nan rock mass (Table 3).

The calculated IOL values range from 26.46 to 34.56, with an average value of 31.81. As can be seen from the S-A-F diagram in Figure 6, the weathering is at the stage of kaolinization, which shows obvious characteristics of desilication, iron-rich and aluminum-rich, indicating a high degree of weathering. CIA values range from 48.68 to 57.26, with an

average value of 53.18. The rock samples are all located near A-CN in the A-CN-K plot, and the weathering process is at the stage of kaolinization, which is consistent with the conclusion presented in the S-A-F diagram.

Table 2. Major elements of surrounding rocks.

No.	Lithology	K2O	Al2O3	CaO	TFe2O3	MgO	SiO2	TiO2	L.O.I	FeO
1	Gabbro	1.13	16.34	8.51	4.71	2.66	58.50	0.99	0.69	2.80
2	Gabbro	1.45	17.21	7.54	8.30	4.74	55.86	0.75	0.31	4.57
3	Gabbro	1.27	16.21	9.07	10.06	6.33	51.81	0.84	0.65	6.43
4	Gabbro	0.76	14.70	10.22	10.26	9.75	51.40	0.49	−0.07	6.47
5	Gabbro	1.16	14.44	9.37	10.03	8.98	52.28	0.68	0.03	6.55
6	Gabbro	0.47	14.65	9.32	10.31	8.89	52.46	0.74	−0.23	7.67
7	Gabbro	0.80	13.42	11.00	10.06	11.20	50.73	0.48	−0.01	7.31
8	Diorite	1.12	17.39	7.91	9.09	6.59	50.14	0.84	2.52	4.86
9	Marble	0.24	3.96	32.40	1.33	10.10	23.86	0.17	28.09	0.08
10	Limestone	0.48	3.70	32.93	2.25	7.92	22.35	0.16	30.52	1.55
11	Domolite	0.05	0.60	31.49	0.16	19.19	4.13	0.03	44.74	0.15

Note: The unit is $\omega(B)/10^{-2}$.

Table 3. The calculation result of chemical weathering index in the study area.

No.	1	2	3	4	5	6	7	8
IOL	34.56	26.46	31.35	33.65	32.69	31.89	32.24	31.64
CIA	56.83	50.75	57.26	54.16	52.10	52.13	53.48	48.72

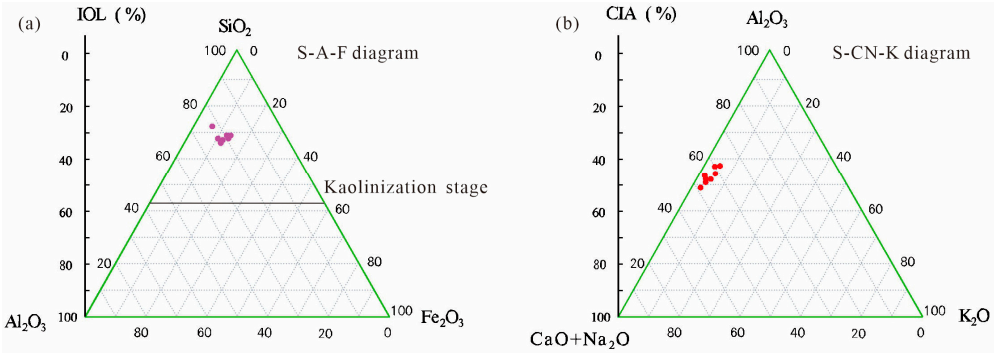

Figure 6. Ternary diagram of IOL and CIA indexes of the rock samples in the study area. (**a**): S-A-F diagram; (**b**): A-CN-K diagram.

4.2.3. Water-Rock Interaction

The weathering and fracture development degree of Ji'nan rock mass present intense, so it could obtain a wide contact area with groundwater and lead to strong water-rock interaction to occur, together with the desilication weathering mechanism, which jointly led the rocks could become intensively leached and supply the source of H_2SiO_3 in the groundwater.

In the study area, the silicate minerals related to the groundwater runoff and occurrence are mainly pyroxene, feldspar, amphibole, etc., whose dissolution can provide not only H_2SiO_3 to the groundwater, but also Ca^{2+}, Mg^{2+} and Na^{+}, etc. It is commonly H_2CO_3 in groundwater that provides solubility, and may also be other acids formed by water-rock interaction or groundwater pollution, such as H_2SO_4 and HNO_3 [25,26].

Correlation analysis between hydrochemical components is often used to reveal the origin relationship between different components [27,28]. As can be seen from the correlation matrix of each chemical component in the groundwater of the study area (Table 4), H_2SiO_3 has a significant positive correlation with SO_4^{-} ($p < 0.01$), and the correlation

coefficient is 0.705, while the correlation coefficient with $H_2CO_3^-$ is only 0.081, showing no correlation, indicating that in the formation process of H_2SiO_3, it is mainly H_2SO_4 involved in the dissolution of silicate minerals, but not H_2CO_3. During the intrusion of the Ji'nan rock mass, the contact zones between Ji'nan rock mass and the previously deposited Cambrian-Ordovician carbonate rocks developed skarn iron ores rich in FeS_2 [29]. In the field, large amounts of pyrite nodules can be seen clearly at the outcrops of this kind of contact zones (Figure 7). With the participation of groundwater, the FeS_2 can be easily oxidized to generate H_2SO_4, which has enhanced the dissolution ability of the groundwater and increased the solubility of the main silicate minerals in Ji'nan rock mass. H_2SiO_3 also presents a significant positive correlation with Ca^{2+} and Mg^{2+} ($p < 0.01$), and the correlation coefficients are respectively 0.635 and 0.696, but poor correlation with Na^+ or K^+ ($p > 0.05$), indicating that the pyroxenes (silicate minerals containing calcium and magnesium) in the study area are the main mineral components providing H_2SiO_3, and albite or potassium feldspars are the secondary mineral components. TDS present a significant positive correlation with H_2SiO_3 ($p < 0.05$), but a negative correlation with HCO_3^-, indicating that the increase of TDS in groundwater is attributed to the dissolution of silicate rocks rather than carbonate rocks. Cations and TDS are negatively correlated with HCO_3^-, indicating that the production of cations inhibited the dissolution of carbonate rocks. As the main carbonate minerals in the study are calcite ($CaCO_3$) and dolomite ($CaMg(CO_3)_2$), it implies that Ca^{2+} and Mg^{2+} produced during the formation of H_2SiO_3 inhibited the dissolution of calcite and dolomite due to the common ion effect. According to the Debye-Hückel Formula, borehole SY12 in the north of the study area was selected randomly to calculate the saturation index of $CaCO_3$ based on the tested hydrochemistry data, the result was $SI_{cal} = 0.36 > 0$, which indicated that groundwater in the north of the study area was saturated with carbonate minerals, which proved that the carbonate deposits were generated due to the common ion effect, and further the content of HCO_3^- became reduced. The main reaction processes involved in these series of water-rock interactions are as follows:

Pyrite oxidizes to produce acid: $4FeS_2 + 15O_2 + 8H_2O \rightarrow 2Fe_2O_3 + 8SO_4^{2-} + 16H^+$ (Sulfuric acid)

Pyroxene dissolution: $H_2SO_4 + Ca(Mg)Al_2Si_2O_8 + 2H_2O \rightarrow Ca^{2+}(Mg^{2+}) + SO_4^{2-} + 2H_2SiO_3 + 2AlOOH$

Table 4. Correlation coefficient matrix of hydrochemical parameters of the groundwater in the study area.

	H_2SiO_3	TDS	Ca^{2+}	Mg^{2+}	Na^+	K^+	HCO_3^-	Cl^-	SO_4^{2-}
H_2SiO_3	1								
TDS	0.463 *	1							
Ca^{2+}	0.635 **	0.951 **	1						
Mg^{2+}	0.696 **	0.905 **	0.986 **	1					
Na^+	0.228	0.948 **	0.806 **	0.726 **	1				
K^+	0.368	0.981 **	0.881 **	0.812 **	0.986 **	1			
HCO_3^-	0.081	−0.396	−0.31	−0.276	−0.431	−0.404	1		
Cl^-	0.2	0.939 **	0.789 **	0.708 **	0.998 **	0.979 **	−0.432	1	
SO_4^{2-}	0.705 **	0.907 **	0.991 **	0.992 **	0.730 **	0.821 **	−0.259	0.708 **	1

Note: ** indicates a significant precorrelation at 0.01 level, and * indicates a significant correlation at 0.05 level.

It is generally believed that with the participation of H_2CO_3, if the H_2SiO_3 in groundwater is mainly sourced from the dissolution of silicate minerals such as feldspar, pyroxene, and amphibole, then $\gamma[(Ca^{2+} + Mg^{2+} + Na^{2+} + K^{2+})/HCO_3^-] = 1.0$, which is called the weathering line of silicate rock [30]. If there are other acids in the water to participate in the dissolution of silicate minerals, the SO_4^{2-}, Cl^- can be provided to participate in the anion balance, and the samples will deviate from the line of $\gamma[(Ca^{2+} + Mg^{2+} + Na^{2+} + K^{2+})/HCO_3^-] = 1.0$. According to the relationship diagram of $\gamma[(Ca^{2+} + Mg^{2+})/HCO_3^-]$ and $\gamma[(Na^+ + K^+)/(HCO_3^-)]$ (Figure 8), it can be seen that the groundwater samples in

the study area are located near or above the weathering line of the silicate rock, indicating that the chemical characteristics of the groundwater in the study area are mainly controlled by the weathering of the silicate rocks and affected by other acids, which is consistent with the conclusion presented in Figure 4. The samples with H_2SiO_3 content greater than 25 mg/L are located above the weathering line of the silicate rocks, and the deviation from the weathering line is large, indicating that the metalicate-rich groundwater is mainly formed by the dissolution of silicate minerals with the participation of other acids. Considering the hydrochemical analysis data of the study area, it indicates that the ionic balance of the groundwater is maintained by SO_4^{2-}. That is, H_2SO_4 is mainly involved in the leaching of silicate minerals. Amounts of samples are located in the region of $\gamma[(Ca^{2+} + Mg^{2+})/HCO_3^-] > 1.0$, indicating that the water environment of the samples has been affected by human activities, which is presumed to be related to the participation of SO_4^{2-} and Cl^- in water ion balance provided by the mining of Zhangmatun Iron Mine on the northeast side of Ji'nan rock mass [31]. The value of $\gamma[(Ca^{2+} + Mg^{2+})/HCO_3^-]$ in all samples was much higher than that of $\gamma[(Na^+ + K^+)/HCO_3^-]$, reflecting that the minerals involved in the leaching process were mostly calcium and magnesia-containing minerals, namely pyroxene in the study area, which was consistent with the above analysis results.

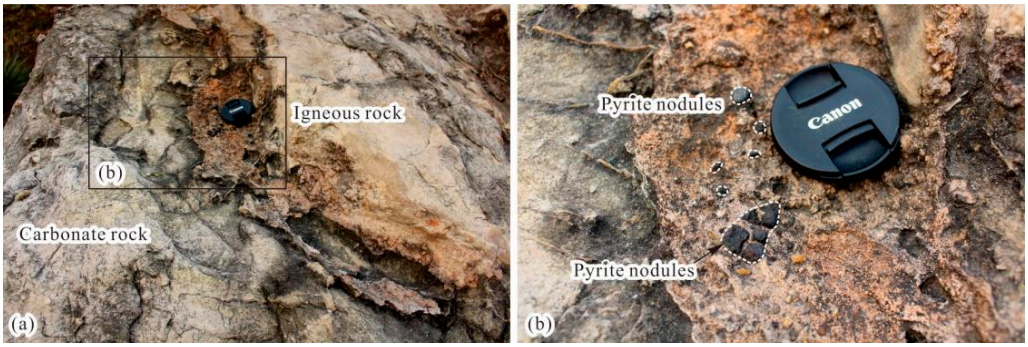

Figure 7. The pyrite nodules developed along the contact zones between the igneous rocks and the surrounding carbonate rocks. (**a**): The contact zone between the igneous rock and the surrounding carbonate rock; (**b**): The pyrite nodules developed along the contact zone.

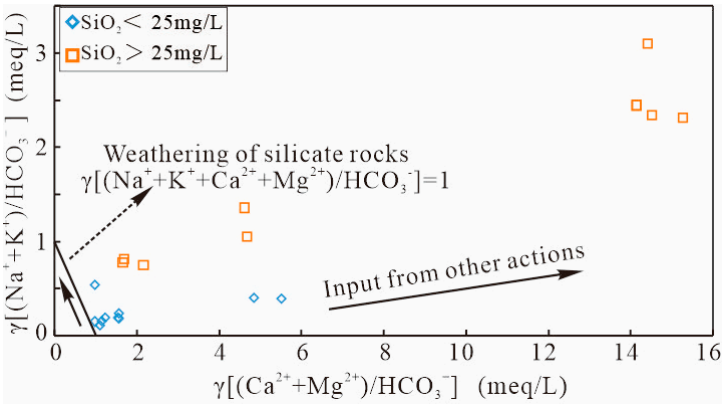

Figure 8. Relative contributions from silicate and carbonate weathering by H_2CO_3.

4.2.4. Conservation and Recharge Conditions of the Groundwater

Influenced by the Yanshan Movement, the terrain of Ji'nan City is high in the south and low in the north, presenting a monoclinic structure. As located in the north of Ji'nan City, the groundwater in the study area can be rapidly recharged by the Wohushan Reservoir, Jinxiuchuan Reservoir and atmospheric precipitation in the southern mountainous area [32]. In addition, the atmospheric precipitation can also rapidly recharge the groundwater along the weak zones, such as the Sangzidian fault, especially the contact zones between

Ji'nan rock mass and the surrounding rocks, along which the FeS_2 could be oxidized to form H_2SO_4, leading the solubility of silicate minerals in groundwater is enhanced. So in the study area, the interaction between atmospheric precipitation, surface water and groundwater is intense, which provided better water source conservation and recharge conditions for the groundwater. As a result, the groundwater runoff is relatively fast, the regeneration rate is quick, and the surrounding rocks or minerals are pretty soluble, thus guaranteeing the enrichment of H_2SiO_3 in groundwater.

The main factors controlling the equilibrium between dissolution and precipitation of the H_2SiO_3 in groundwater are the supply source of metasilicate minerals (solid amorphous SiO_2) and the solubility of secondary minerals formed during weathering. Through the equilibrium system of dissolution-precipitation of metasilicate minerals, not only can we identify the source of H_2SiO_3, but also can indicate the relative saturation of metasilicate minerals in the groundwater, and then help judge the solubility of metasilicate minerals in the groundwater [30]. As shown in Figure 9, in the $[Na^+]/[H^+]$-H_2SiO_3 system (Figure 9a), the groundwater sample points in the study area are generally located in the stable area of kaolinite, indicating that the water-rock interaction is in the process of forming kaolinite by the inhomogeneous dissolution of plagioclase, which is consistent with the above analysis that the rock weathering is mostly at the stage of kaolinization (CIA, IOL) (Figure 6). In the system of $[Mg^{2+}]/[H^+]$-H_2SiO_3 (Figure 9b), the samples are generally located in the stable end-member of chlorite, and some samples with SiO_2 < 25 mg/L are located in the stable end-member of kaolinite. In the $[Ca^{2+}]/[H^+]$-H_2SiO_3 system (Figure 9c), all the samples are located in the stable end-member of kaolinite. All the groundwater samples did not reach the saturation state of metasilicate minerals, indicating that all the samples have the ability to continue to dissolve metasilicate minerals, which reflected that the groundwater in the study area was rapidly recharged so that it could maintain the persistent ability to dissolve the metasilicate minerals.

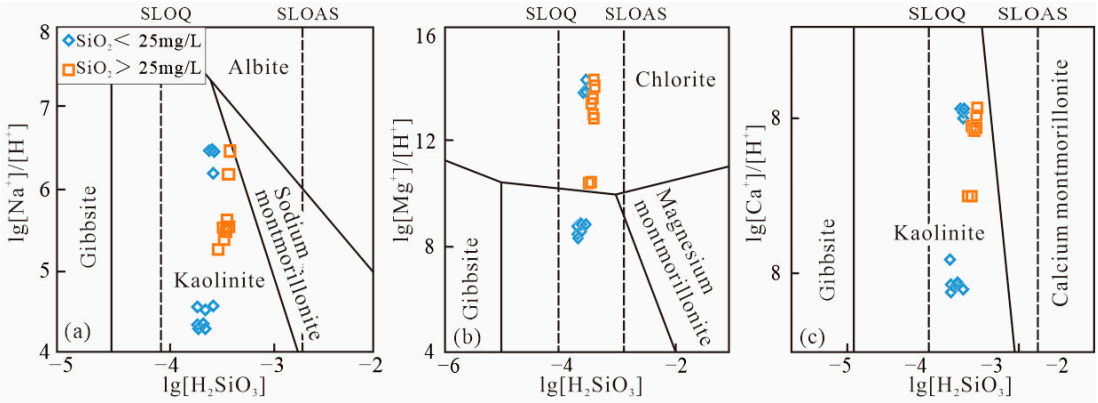

Figure 9. Mineral equilibrium phase diagram for the groundwater in the study area. SLOQ = saturation line of quartz; SLOAS = saturation line of amorphous SiO_2. (**a**): the $[Na^+]/[H^+]$-H_2SiO_3 system; (**b**): the $[Mg^{2+}]/[H^+]$-H_2SiO_3 system; (**c**): the $[Ca^{2+}]/[H^+]$-H_2SiO_3 system.

4.3. Genetic Model of the Metasilicate Enrichment

Based on the spatial distribution characteristics and hydrogeological conditions of metasilicate-rich groundwater in the Ji'nan rock mass area obtained by the above research, and combined with the genetic mechanism of the Ji'nan spring area analyzed by previous scholars [33,34], the causes of the enrichment of H_2SiO_3 in groundwater in the study area are summarized as the following: After the infiltration of atmospheric precipitation, the water flew from south to north through the Ordovician limestone. During the runoff process, parts of the water got blocked by the Ji'nan rock mass and then migrated upward to form Baotu Spring, Heihu Spring, etc., and parts of the water entered the deep circulation, and participated in the strong water-rock interaction along the weathering zones of the rock mass, the weak zones of fractures, and especially the contact zones between Ji'nan rock mass

and surrounding rocks, where the FeS_2 were oxidized to produce amounts of H_2SO_4 in groundwater, making the groundwater in the study area present strong dissolution ability. The metasilicate minerals such as pyroxene, plagioclase, and amphibole in the silicate rocks were dissolved and desilicated, and the silicon elements entered the groundwater and moved along the runoff direction of the groundwater, and finally accumulated in the downstream of Ji'nan rock mass (i.e., the north side of Ji'nan rock mass), which led to the enrichment of H_2SiO_3 in groundwater (Figure 10). However, on the northeast side of Ji'nan rock mass, there are human production activities such as the mining of Zhangmatun Iron Mine [31], which caused sulfur pollution to the groundwater and further inhibited the dissolution of silicate minerals, so the water-rock interaction became weakened, resulting only part of the sample sites developed the metasilicate-rich groundwater in this area. More samples would be more beneficial to conclude the reliable genetic model.

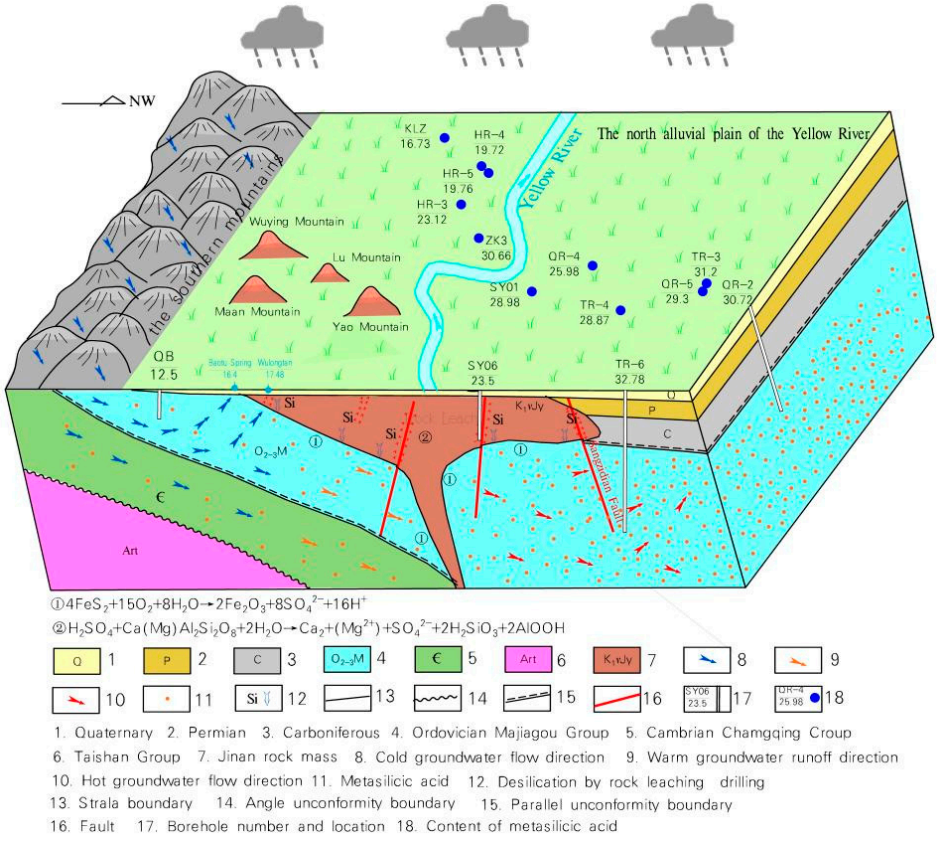

Figure 10. Genetic model of the metasilicate-rich groundwater around Ji'nan rock mass.

5. Conclusions

(1) The distribution of the metasilicate-rich groundwater in the Ji'nan rock mass area was spatially different. On the northwest side and part of the northeast side, the content of H_2SiO_3 in groundwater was large, forming metasilicate-rich groundwater. However, on the east, west, and south sides of the rock mass, little metasilicate-rich groundwater developed.

(2) Ji'nan rock mass is mainly composed of gabbro and contains amounts of silicate minerals that easily weathered. The weathering was at the stage of kaolinization showing a high degree, and presented the desilication mechanism, which acted as the main source of H_2SiO_3 in the groundwater.

(3) FeS_2 developed along the contact zones between the Ji'nan rock mass and surrounding rocks, which were easily oxidized to produce H_2SO_4 and enhanced the ability of groundwater to dissolve silicate minerals. The study area is located at the low position of the monocline structure, where the groundwater could be recharged and renewed quickly.

(4) Lithology, structure and hydrochemical characteristics constitute the favorable factors for the formation of metasilica-rich groundwater, whereas, sulfur pollution caused by human activities acted as the negative factor. In the future, more samples are suggested to be collected and tested, in order to verify the controlling factors and make up the genetic model.

Author Contributions: Conceptualization, L.Z.; methodology, C.H.; software, S.Y. and J.S.; validation, G.S.; formal analysis, M.X.; investigation, M.X.; resources, W.P.; data curation, W.P.; writing—original draft preparation, M.X.; writing—review and editing, M.X. and C.H.; visualization, G.S.; supervision, L.Z.; project administration, C.H.; funding acquisition, G.S. All authors have read and agreed to the published version of the manuscript.

Funding: This research was funded by National Natural Science Foundation of China, grant number 42002127.

Data Availability Statement: Not applicable.

Conflicts of Interest: The authors declare no conflict of interest.

References

1. Wada, Y.; Flörke, M.; Hanasaki, N.; Eisner, S.; Fischer, G.; Tramberend, S.; Satoh, Y.; Van Vliet, M.T.H.; Yillia, P.; Ringler, C.; et al. Modeling Global Water Use for the 21st Century: The Water Futures and Solutions (WFaS) Initiative and Its Approaches. *Geosci. Model Dev.* **2016**, *9*, 175–222. [CrossRef]
2. Liu, Y.Q.; Wen, D.G.; Lü, L.; Li, W.; Zhang, F.C.; Wang, X.F.; Meng, S.X. Characteristics of karst groundwater flow systems of typical faulted basins in Yimeng Mountain area: A case study of Laiwu Basin. *Bull. Geol. Sci. Technol.* **2022**, *41*, 157–167.
3. Xiao, Y.; Hao, Q.C.; Zhang, Y.H.; Zhu, Y.C.; Yin, S.Y.; Qin, L.M.; Li, X.H. Investigating sources, driving forces and potential health risks of nitrate and fluoride in groundwater of a typical alluvial fan plain. *Sci. Total Environ.* **2022**, *802*, 149909. [CrossRef]
4. McDonald, R.I.; Green, P.; Balk, D.; Fekete, B.M.; Revenga, C.; Todd, M.; Montgomery, M. Urban Growth, Climate Change, and Freshwater Availability. *Proc. Natl. Acad. Sci. USA* **2011**, *108*, 6312–6317. [CrossRef]
5. Polemio, M.; Voudouris, K. Groundwater Resources Management: Reconciling Demand, High Quality Resources and Sustainability. *Water* **2022**, *14*, 2107. [CrossRef]
6. Xiao, Y.; Liu, K.; Hao, Q.C.; Li, Y.S.; Xiao, D.; Zhang, Y.J. Occurrence, Controlling Factors and Health Hazards of Fluoride Enriched Groundwater in the Lower Flood Plain of Yellow River, Northern China. *Expo. Health* **2022**, *14*, 345–358. [CrossRef]
7. Xiao, Y.; Liu, K.; Hao, Q.C.; Xiao, D.; Zhu, Y.C.; Yin, S.Y.; Zhang, Y.H. Hydrogeochemical insights into the signatures, genesis and sustainable perspective of nitrate enriched groundwater in the piedmont of Hutuo watershed, China. *Catena* **2022**, *212*, 106020. [CrossRef]
8. Zhou, C.S.; Zou, S.Z.; Zhu, D.N.; Lin, Y.S.; Wang, J.; Fan, L.J.; Li, J.; Lan, F.N.; Li, Y.Q.; Deng, R.X.; et al. Characteristics, causes and development suggestions of high quality groundwater containing metasilicate in Zhaojue area, Sichuan Province. *Geol. China* **2022**, *49*, 849–859.
9. Kim, S.H.; Choi, B.Y.; Lee, G.Y.; Yun, S.T.; Kim, S.O. Compositional data analysis and geochemical modeling of CO2- water- rock interactions in three provinces of Korea. *Environ. Geochem. Health* **2019**, *41*, 357–380. [CrossRef]
10. Sun, Q.F.; Tian, H.; Guo, X.D.; Yu, H.M.; Li, L.J. The discovery of silicic acid and strontium enrichment areas in groundwater of Changchun area, Jilin Province. *Geol. China* **2017**, *44*, 1031–1032.
11. Sun, H.Y.; Wei, X.F.; Sun, X.M.; Jia, F.C.; Li, D.J.; He, Z.X.; Li, J. Formation mechanism and geological construction constraints of metasilicate mineral water in Yudaokou, Hannuoba basalt area. *Earth Sci.* **2020**, *45*, 4236–4253.
12. Li, C.S.; Wu, X.C.; Sun, B.; Sui, H.B.; Geng, F.Q.; Qi, H.; Ma, X.Y. Hydrochemical characteristics and formation mechanism of geothermal water in northern Ji'nan. *Earth Sci.* **2018**, *43*, 313–325.
13. Wang, S.J.; Zhang, C.J.; Yang, E.X.; Song, Z.Y.; Wang, L.F.; Xu, K.M. Division of Mesozoic intrusive stages in Luxi area. *Shandong Land Resour.* **2009**, *25*, 18–23.
14. Shan, T.T.; Xu, S.G.; Fan, Z.G.; Ruan, W. Characteristics and formation mechanism of metasilicate mineral water in Xishan mountain of Kunming. *J. Kunming Univ. Sci. Technol.* **2019**, *44*, 39–47.
15. Sun, H.Y.; Sun, X.M.; Wei, X.F.; Chen, Z.R.; Liu, W.; Huang, X.K.; Li, X.; Yin, Z.Q.; Liu, W.B. Formation mechanisms of metasilicate mineral water in Chengde, Hebei Province: Evidence from rock weathering and water-rock interaction. *Geol. China* **2022**, *49*, 1088–1113.
16. Ye, N.; Li, Y.T.; Huang, B.W.; Xi, B.B.; Jiang, H.; Lu, Z.Y.; Chen, Q.L.; You, D.H.; Xu, J. Hydrothermal silicification and its impact on Lower–Middle Ordovician carbonates in Shunnan area, Tarim Basin, NW China. *Geol. J.* **2022**, *57*, 3538–3557. [CrossRef]
17. Liang, C.C.; Wang, W.; Ke, X.M.; Ou, A.F.; Wang, D.H. Hydrochemical Characteristics and Formation Mechanism of Strontium-Rich Groundwater in Tianjiazhai, Fugu, China. *Water* **2022**, *14*, 1874. [CrossRef]
18. Moses, C.; Robinson, D.; Barlow, J. Methods for measuring rock surface weathering and erosion: A critical review. *Earth-Sci. Rev.* **2014**, *135*, 141–161. [CrossRef]

19. Wu, B.J.; Peng, B.; Zhang, K.; Kuang, X.L.; Fang, X.H.; Zeng, D.Z. A new chemical index of identifying the weathering degree of black shales. *Acta Geol. Sin.* **2016**, *90*, 818–832.
20. Ofili, S.; Soesoo, A.; Panova, E.G.; Hints, R.; Hade, S. Geochemical Reconstruction of the Provenance, Tectonic Setting and Paleoweathering of Lower Paleozoic Black Shales from Northern Europe. *Minerals* **2022**, *12*, 602. [CrossRef]
21. Nesbitt, H.W.; Young, G.M. Early Proterozoic climates and plate motions inferred from major element chemistry of lutites. *Nature* **1982**, *299*, 715–717. [CrossRef]
22. Babechuk, M.G.; Widdowson, M.; Kamber, B.S. Quantifying chemical weathering intensity and trace element release from two contrasting basalt profiles, Deccan Traps, India. *Chem. Geol.* **2014**, *363*, 56–75. [CrossRef]
23. Romero-Mujalli, G.; Hartmann, J.; Hosono, T.; Louvat, P.; Okamura, K.; Delmelle, P.; Amann, T.; Böttcher, M.E. Hydrothermal and magmatic contributions to surface waters in the Aso caldera, southern Japan: Implications for weathering processes in volcanic area. *Chem. Geol.* **2022**, *588*, 120612. [CrossRef]
24. Rouzaut, S.; Campodonico, V.A.; Pasquini, A.I. Weathering and paleoprecipitation indices in a Late Pleistocene–Holocene loess–paleosol sequence in central Argentina. *Environ. Earth Sci.* **2021**, *80*, 28. [CrossRef]
25. Gao, Z.J.; Wang, Z.S.; He, K.Q.; Victor, K.; Liu, J.T. Hydrochemical characteristics and controlling factors of karst groundwater in middle and upper reaches of Dawen River basin. *Bull. Geol. Sci. Technol.* **2022**, *41*, 264–272.
26. Hu, X.B.; Fang, J.C.; Zhai, H.W.; Zhang, K.; Ma, Y.M.; Jin, J.H.; Gao, X.B. Application of sulfur and oxygen isotopes in identifying the source of sulfate in karst water from Xin'an spring area. *Bull. Geol. Sci. Technol.* **2022**, *41*, 333–340.
27. Kale, A.; Bandela, N.; Kulkarni, J.; Sahoo, S.K.; Kumar, A. Hydrogeochemistry and multivariate statistical analysis of groundwater quality of hard rock aquifers from Deccan trap basalt in Western India. *Environ. Earth Sci.* **2021**, *80*, 288. [CrossRef]
28. Liu, P.; Yang, M.; Sun, Y.J. Hydro-geochemical processes of the deep Ordovician groundwater in a coal mining area, Xuzhou, China. *Hydrogeol. J.* **2019**, *27*, 2231–2244. [CrossRef]
29. Deng, J.; Wang, C.M.; Bagas, L.; Santosh, M.; Yao, E.Y. Crustal architecture and metallogenesis in the south-eastern North China Craton. *Earth-Sci. Rev.* **2018**, *182*, 251–272. [CrossRef]
30. Guo, Q.H.; Wang, Y.X. Simulation of geochemical processes affecting groundwater in Quaternary porous aquifers of Taiyuan basin: A typical Cenozoic rift basin. *Earth Sci. Front.* **2014**, *21*, 83–90.
31. Wang, H.H.; Li, X.Z.; Shen, L.J.; Zhu, Y.Z.; Zhou, M.L. Geological characteristics and metallogenic model of "Yucheng Type" rich ion deposit in Qihe Yucheng area in Shandong Province. *Shandong Land Resour.* **2021**, *37*, 26–35.
32. Jia, C.; Wang, C.; Liu, S.; Yang, X.; Liu, W.; Gao, S.; Zhu, H.H. Study on hydrogeochemical characteristics of groundwater in the alluvial plain of western Ji'nan. *Water Resour. Hydropower Eng.* **2022**, *53*, 49–60.
33. Wang, J.L.; Jin, M.G.; Lu, G.P.; Zhang, D.L.; Kang, F.X.; Jia, B.J. Investigation of discharge-area groundwaters for recharge source characterization on different scales: The case of Ji'nan in northern China. *Hydrogeol. J.* **2016**, *24*, 1723–1737. [CrossRef]
34. Xing, L.T.; Yu, M.; Su, Q.W.; Zhao, Z.H.; Gao, Y.; Zhang, Y.F. Influence and repair of underground engineering construction on karst flow field. *Bull. Geol. Sci. Technol.* **2022**, *41*, 242–254.